Reconstructing chaotic dynamics through spike filters

Rolando Castro[1] and Tim Sauer[2]
[1]*Colegio Universitario de Humacao, Estación Postal CUH, Departamento de Matemáticas Computacionales, 100 Carretera 908, Humacao, Puerto Rico 00791*
[2]*Institute of Computational Sciences and Informatics and Department of Mathematical Sciences, George Mason University, Fairfax, Virginia 22030*
(Received 31 July 1998)

We consider the problem of reconstructing chaotic attractors from spike trains produced by model neurons. We find that the period-parameter plot, which displays the dependence of the oscillation frequency of the spiking model on the input level, is a useful device for determining the success of reconstruction. A three-dimensional version of Fitzhugh-Nagumo spiking dynamics is investigated along with other models. [S1063-651X(99)11103-6]

PACS number(s): 05.45.−a, 05.40.−a, 87.10.+e, 87.19.La

I. INTRODUCTION

In most experimental situations the differential equations for the system under investigation and, consequently, the state variables, are unknown. The experimenter may have access to consecutive measurements of only a single scalar observable. A considerable step forward was made when it was shown that the attractor of the underlying system can be reconstructed from such a time series by a procedure called time delay embedding [1–3]. This result is especially useful for nonlinear systems, where the potential exists for extremely complicated state space attractors.

Neurons communicate by sequences of short pulses, the so-called action potentials or spikes. The times of these discrete pulses can be collected by a recording electrode. This type of data differs from a time series of an observable measured at regular time intervals. Many hypotheses and neuron models for the description of these pulses have been proposed, including integrate-and-fire (IF) models and models of excitable media [4–10].

In [11,12] the question of whether the attractor of a chaotic input can be reconstructed from delay embeddings of the interspike intervals (ISIs) generated by a neuron model was considered. It was shown in [11] that it is possible by using a simple integrate-and-fire neuron model. In [12], Racicot and Longtin investigated the ISIs generated from three integrate-and-fire models and an excitable model [FitzHugh-Nagumo (FHN2) model [9]]. Attractors constructed from delay embeddings of ISIs and of the chaotic input were compared from the point of view of geometry and nonlinear forecastability. They found that for the IF models the similarity between these attractors is high only when the mean firing rate (mean number of spikes per unit of time) is high, and when firings occur over a large range of the input signal. For the more complicated excitable FHN2 model, good reconstructions were not reported, and the ISIs reconstructions bear little resemblance to the input attractor.

The focus of this short paper is to isolate the factors necessary for successful ISI reconstructions in practice. We show that the period-parameter plot, which displays the dependence of the oscillation frequency of the spiking model on the input level, can be used to determine the success of reconstruction for various input ranges. In particular, we can explain the reason of the difficulty reported in [12] with reconstructing through the FHN2 filter and show that readjusting the input range to FHN2 can solve this problem.

This paper is organized as follows. The definition of the period-parameter plot and its relation with attractor reconstruction via neuron filters is the subject of Sec. II. We introduce a version of the FitzHugh-Nagumo model that typically allows faithful reconstruction from spike trains. In Sec. III the predictability of the spike train is introduced as a measure of reconstruction success, using a nonlinear forecasting method and surrogate data as a statistical control. The Hodgkin and Huxley neuron model [10] is studied in Sec. IV.

II. THE PERIOD/PARAMETER PLOT

In 1962, FitzHugh and Nagumo [9] proposed a simple model that gives a descriptive portrait of neural excitation without direct reference to known or conjectured physiological variables. It has played an important role in leading to an understanding of the nature of excitable systems (where a stimulus larger than some threshold will provoke a very large response) and in studying more complicated models of the action potentials. The FHN2 model equations are

$$\begin{aligned} \epsilon \dot{v} &= -v(v-a)(v-1)-w+S(t), \\ \dot{w} &= v-w-b, \end{aligned} \tag{1}$$

where v is the fast or excitation variable which mimics the action potentials, w is the slow or recovery variable which determines the refractory time (during which an action potential cannot be generated), and $S(t)$ is the applied stimulus that leads to excitation. We used the parameter values $a=0.5$, $b=0.15$, $\epsilon=0.005$. For these parameter values there is a globally stable fixed point if $S\equiv 0$, i.e., without an input signal. For a constant input signal, $S(t)\equiv S$, the system has an equilibrium at $(v,w)=(v_0,v_0-b)$, where v_0 is a real-valued root of $v_0(v_0-a)(v_0-1)=S+b-v_0$. For $S(t)\equiv S$, a sufficiently large constant parameter, the equilibrium becomes unstable and a stable periodic orbit is generated.

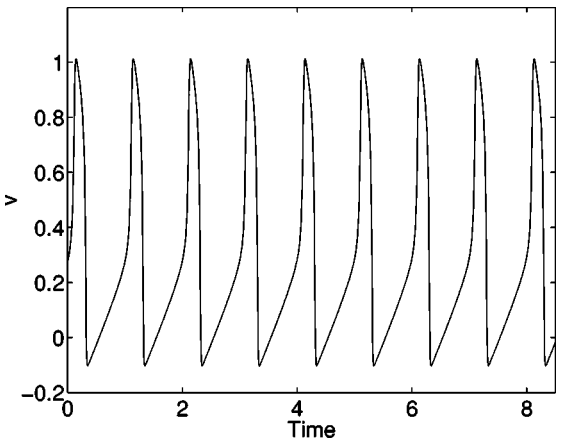

FIG. 1. The FHN2 model exhibits periodic spiking behavior of the voltage v for $S>S_H$ $(S=0.2)$.

The periodic orbit is manifested in rhythmical spiking by the variable v (Fig. 1). For the parameters chosen there is a supercritical Hopf bifurcation point at $S_H \approx 0.112\,331\ldots$. An alteration in the FHN2 model yields a new model (FHN3) [13] with the same property [if $S(t)$ is set to be a constant input signal S, there is a Hopf bifurcation as S is increased]. The FHN3 equations are

$$\dot{u} = -au - cw + S(t),$$

$$\epsilon\dot{v} = -v(v-b)(v-1) + u - dw, \tag{2}$$

$$\dot{w} = v^2 - w - b,$$

where the parameters are set to be $a=0.1$, $b=0.15$, $c=0.5$, $d=0.5$, $\epsilon=0.005$ (bifurcation point is $S_H \approx -0.053$).

Figure 2 shows period-parameter plots for FHN2 and FHN3 models, a plot of the periods of the periodic orbit created by the Hopf bifurcation versus the constant input signal S for these models. The purpose of the period-parameter plot is to find a range of the fixed input parameter S over which the spiking period is a monotonic function of S. If the applied stimulus $S(t)$ is restricted to this monotonic range, the output spikes can distinguish between different stimulus intensities, and relay information about the stimulus signal. Figure 2 shows that the interval $-0.05 \leqslant S \leqslant 0.05$ is a *monotonic input range* for FHN3. Note that the FHN2 curve is relatively flat, which is not the case for the FHN3 curve. Therefore, the spike train output of FHN3 will be able to distinguish different inputs better than FHN2.

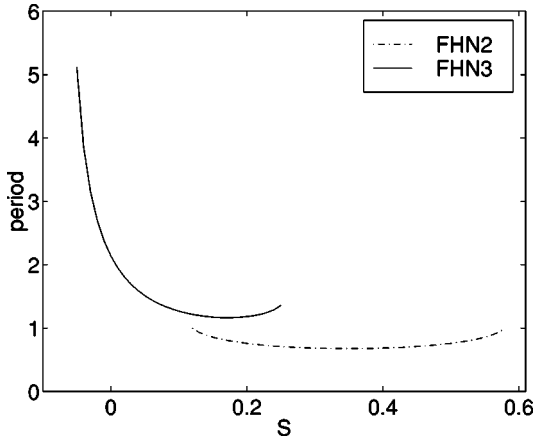

FIG. 2. Period-parameter plots for the FHN2 and FHN3 models subject to a constant input S. The range of S over which the spiking period is monotonic provides a scaling range to the input of the neuron models where good reconstructions are obtained.

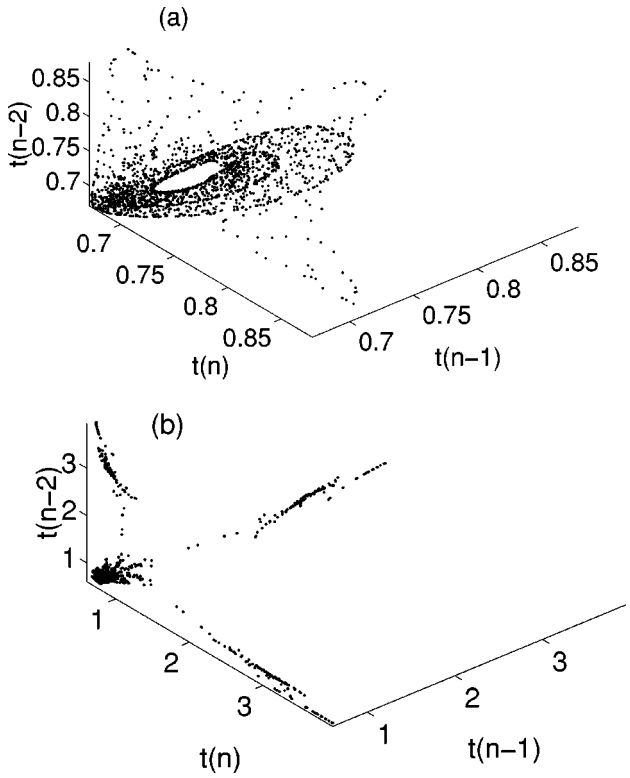

FIG. 3. Plots of 3-tuples of the ISIs generated with the FHN2 model using a scaled version of the x coordinate of the Rössler equations as the input. Parameters used: $\tau=0.5$, $A=0.36$, $B=0.4$, $C=4.5$. (a) The input signal used is $S(t)=0.007\,292x(t)+0.2483$ which scales the x variable to the monotonic input range $[0.19,\ 0.33]$. (b) The input signal used is $S(t)=0.026\,042x(t)+0.4083$ which scales the x variable to the nonmonotonic input range $[0.2, 0.7]$.

If the range of the applied stimulus $S(t)$ to the neuron model is not contained in a domain of monotonicity of the neuron model, then the information about the stimulus $S(t)$ will not be efficiently carried in the spike train output. To illustrate this point, we generate chaotic inputs to the neuron models using the Rössler [14] and the Lorenz equations [15]. The Lorenz attractor has a figure eight shape; the Rössler attractor has a funnel shape and a banded structure. Figure 3 shows the delay embedding of the ISIs generated with the FHN2 model and a scaled version of the x variable of the Rössler system as the input $S(t)$ to the neuron model. The Rössler equations are $\dot{x} = -y - z$, $\dot{y} = x + Ay$, $\dot{z} = B + (x - C)z$, with parameter values $A=0.36$, $B=0.4$, $C=4.5$.

Spiking times were determined by numerically integrating the coupled Rössler and FHN2 equation,

$$\begin{aligned}\dot{x} &= \tau(-y-z),\\ \dot{y} &= \tau(x+Ay),\\ \dot{z} &= \tau(B+(x-C)z),\\ \epsilon\dot{v} &= -v(v-a)(v-1)-w+S(t),\\ \dot{w} &= v-w-b,\end{aligned} \tag{3}$$

and by finding the times (called firing times) at which the variable v makes positive-going crossings of a fixed threshold (arbitrarily set to 0.7). The ISIs are defined by $t_n = T_{n+1} - T_n$, where T_n and T_{n+1} are consecutive firing times. Figure 3(a) shows the ISI attractor generated when a monotonic input range was used. We used the input signal $S(t) = 0.007\,292x(t) + 0.2483$ and plot the vectors (t_n, t_{n-1}, t_{n-2}). This input signal results in an input range $0.19 \leqslant S(t) \leqslant 0.33$. Note that the attractor reconstructed by ISIs resembles the Rössler attractor. For Fig. 3(b) we used the input signal $S(t) = 0.026\,042x(t) + 0.4083$ which produces an input range of $0.2 \leqslant S(t) \leqslant 0.7$. This input range is not monotonic, as can be seen from Fig. 2, and as a result the attractor was poorly reconstructed. Similarly, in [12] the input used for the FHN2 model did not fall in a monotonic input range and successful reconstructions were not reported.

Figure 4 shows the delay embedding of the ISIs generated with the FHN3 model and a scaled version of the x variable of the Lorenz system as the input. The Lorenz equations are $\dot{x} = \alpha(y-x)$, $\dot{y} = \rho x - y - xz$, $\dot{z} = -\beta z + xy$ with parameter values $\alpha = 10$, $\rho = 28$, $\beta = 8/3$. Spiking times were determined as above by numerically integrating the coupled Lorenz and FHN3 equations

$$\begin{aligned}\dot{x} &= \tau(\alpha(y-x)),\\ \dot{y} &= \tau(\rho x - y - xz),\\ \dot{z} &= \tau(-\beta z + xy),\\ \dot{u} &= -au - cw + S(t),\\ \epsilon\dot{v} &= -v(v-b)(v-1) + u - dw,\\ \dot{w} &= v^2 - w - b.\end{aligned} \tag{4}$$

A monotonic input range was used in Fig. 4(a) [$S(t) = 0.003\,75x(t) + 0.075$, $0 \leqslant S(t) \leqslant 0.15$]. Note that the attractor has the figure eight shape of the Lorenz attractor. For Fig. 4(b) we used a nonmonotonic input range of $-0.15 \leqslant S(t) \leqslant 0.15$ produced by the input signal $S(t) = 0.0075x(t)$. The bifurcation point of the FHN3 model is contained in that range. Note that the quality of reconstruction degrades.

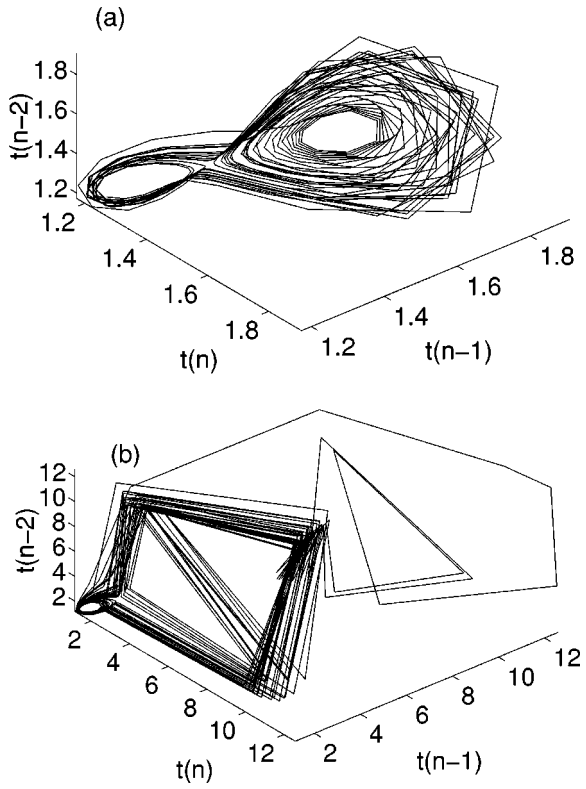

FIG. 4. Plots of 3-tuples of the ISIs generated with the FHN3 model using a scaled version of the x coordinate of the Lorenz equations as the input. Parameters used: $\tau = 0.05$, $\alpha = 10$, $\rho = 28$, $\beta = 8/3$. (a) The input signal used is $S(t) = 0.003\,75x(t) + 0.075$ which scales the x variable to the monotonic input range $[0, 0.15]$. (b) The input signal used is $S(t) = 0.0075x(t)$ which scales the x variable to the nonmonotonic input range $[-0.15, 0.15]$.

III. NONLINEAR PREDICTION

The preceding section showed visual comparison of attractor reconstruction through interspike interval information. A more objective measure of the success of a reconstruction can be given by measuring the predictability of the spike train, using the geometry of the reconstructed attractor. Nonlinear forecastability is an intrinsic property of a deterministic dynamical system [16]. We will use a simple version of a nearest-neighbor prediction algorithm [11,17,18] to measure predictability. The prediction algorithm works as follows. An m-dimensional delay embedding is constructed from a sequence of ISIs $(t_1, t_2, t_3, \ldots, t_N)$ in the same way as for a time series [16] yielding vectors of the form $V_n = (t_n, \ldots, t_{n-m+1})$. For each V_n, the k nearest neighbors $V_n^j = (t_n^j, \ldots, t_{n-m+1}^j)$, $j = 1 \ldots k$, are collected (we used $k = 10\%$ of N for the calculations in this paper). To avoid biasing predictions by in-sample interpolation, the nearest neighbors close in time to V_n are not selected. The nearest neighbors chosen are translated by the horizon h, and the average

$$p_n = \frac{1}{k}\sum_{j=1}^{k} t_{j+h}^j$$

is used to approximate the future interval t_{n+h}. The difference $e_n^p = p_n - t_{n+h}$ is the h-step prediction error at step n.

We could instead use the series mean M to predict at each step; this h-step prediction error is $e_n^M = M - t_{n+h}$. The ratio of the root-mean-square errors of the two possibilities (the nonlinear prediction algorithm and the constant prediction of the mean) gives a normalized prediction error of $\langle (e_n^p)^2 \rangle^{1/2} / \langle (e_n^M)^2 \rangle^{1/2}$, where the averages are taken over the entire series. An NPE value close to 1 means low predictability, with M being the best forecast. An NPE value close to zero means high predictability (linear or nonlinear) in the ISI sequence.

We generate sequences of 3000 ISIs and compute the one-step-ahead prediction error using embedding dimension $m=3$. A sequence of ISIs generated as in Fig. 4(a), for instance, yields a very low NPE of 0.076, reflecting again a successful reconstruction. Since linear correlations can fool the nonlinear prediction algorithm [19,20] by giving small NPE values, we used the surrogate data method [21] to check the nature of the correlations in the ISI sequences.

The surrogate data method works as follows. A linear process is specified as a null hypothesis; data sets (called surrogates) which are consistent with this null hypothesis are generated. The surrogate data have similar properties as the original ISIs but is a realization of a stochastic process. A discriminating statistic (NPE in our case) is computed for the original and for each of the surrogate data sets. The null hypothesis is rejected (nonlinearity is detected) if the statistic computed for the original data is significantly different than the ensemble of values computed for the surrogate data. This method has been used to validate dimension measurements and to discriminate deterministic versus stochastic dynamics from neuronal data [18]. Two types of surrogate data are used in our analysis, phase-randomized (PR) and Gaussian-scaled (GS) surrogate. The PR surrogate has the same mean, standard deviation, and autocorrelation as the original ISI series, but is the realization of a Gaussian stochastic process. The nonlinear deterministic structure is eliminated. The GS surrogate (also known as amplitude-adjusted phase-randomized surrogate) corresponds to the hypothesis that the ISI series is a monotonically scaled version of amplitudes produced by a Gaussian random process with similar autocorrrelation.

From each ISI sequence of interest we generate ten surrogate sets of each of the two types of surrogate. The NPEs for each type are averaged together and are compared with the NPE of the original ISI sequence. If the NPE of the original sequence is significantly different from the NPEs of the surrogates, the null hypothesis of the surrogates can be rejected, which is evidence that the nonlinear structure of the underlying dynamical system is present in the interspike intervals.

Figure 5 shows the plot of the NPE (one-step-ahead) values of a sequence of 3000 ISIs (lower curve) and the mean of the NPEs of the surrogates (upper curves) versus the embedding dimension m. The error bar denotes two standard deviations. The ISIs were generated using the FHN3 model and the Lorenz equations [see Fig. 4(a)]. Note that for each m, the NPEs of the ISIs (lower curve) are significantly different from the NPEs of the surrogates, therefore there is predictability not explained by any of the null hypotheses controlled by the surrogate data. We can conclude that there is predictability in the ISI series caused by the underlying deterministic dynamics. Figure 6 shows the plot of the NPEs as a function of the prediction horizon h (lower curve for the ISI data and upper curves for its surrogates). For these calculations we fixed the embedding dimension $m=3$. For each prediction horizon there is a statistically significant difference between the original series and its surrogates; again the null hypotheses can be rejected.

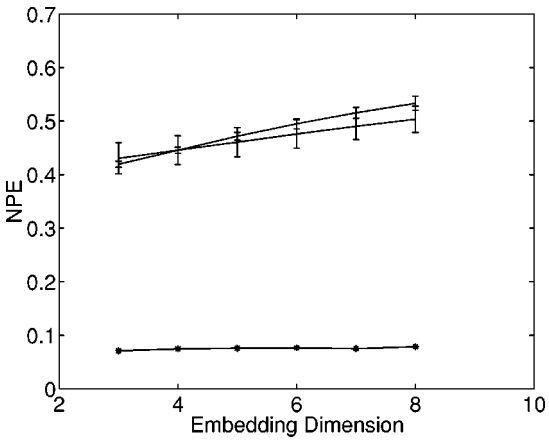

FIG. 5. Normalized one-step-ahead prediction error for ISIs created with the FHN3 model and the Lorenz equations [as in Fig. 4(a)] and two different types of surrogate data (phase-randomized surrogates, Gaussian-scaled surrogates). The lower curve is the NPE for the ISIs, the upper curves are for the mean NPE for 10 surrogates of each type. The error bars denote two standard deviations.

An important issue to be considered in the reconstruction analysis is the relative time scales of the input stimulus oscillations and the spiking model, which is determined by a parameter τ in our analysis. Reducing τ has the effect of slowing the dynamics of the stimulus. The theoretical limit $\tau \to 0$ corresponds to a fixed input activity level, at which point the spiking filter acts as an amplitude-to-frequency converter, a faithful conversion which will invert though preserve dynamical information. Because of this we should expect more successful reconstruction for small τ. For this analysis we used the FHN2 model with a scaled version of

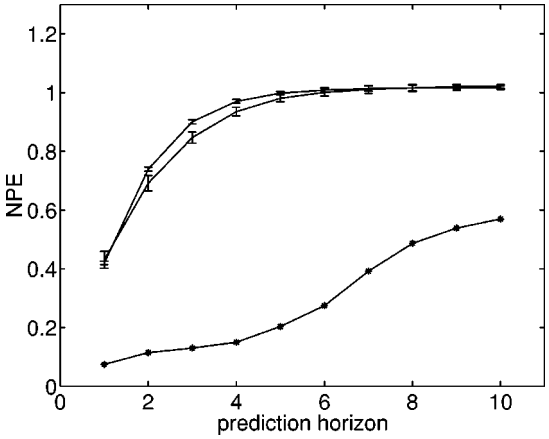

FIG. 6. NPE ($m=3$) as a function of prediction horizon. The lower curve is the NPE for the ISIs created as in Fig. 4(a); upper curves are the mean NPEs of ten surrogates sets (phase-randomized surrogates, Gaussian-scaled surrogates). The error bars denote two standard deviations.

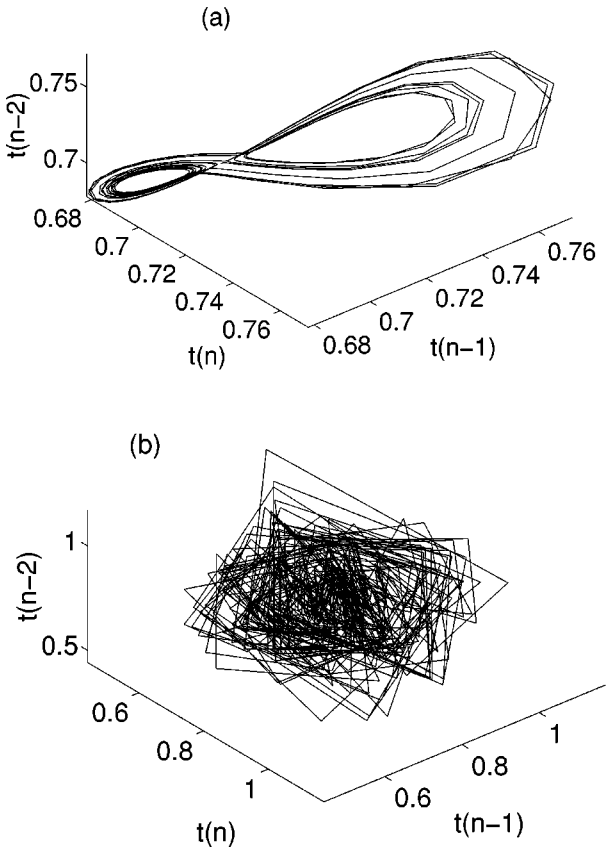

FIG. 7. Plots of 3-tuples of the interspike intervals generated with the FHN2 model using a scaled version of the x coordinate of the Lorenz equations as the monotonic input range, $S(t)=0.0035x(t)+0.26$: (a) $\tau=0.05$, (b) $\tau=1$.

the x coordinate of the Lorenz equations as the input to the model. Figure 7 shows the ISI attractor generated using two different values of τ and the same input signal $S(t)=0.0035x(t)+0.26$. We get a good reconstruction for $\tau=0.05$, the ISI attractor has the figure eight shape of the Lorenz attractor, and a sequence of 3000 ISIs yields an NPE of 0.092 ($h=1$, $m=3$). For $\tau=1$, the attractor is poorly reconstructed. To study the effect of τ in the reconstruction, we generate ISI sequences using different τ values and compute the NPEs (one step ahead, $m=3$) for each of them. To compare different τ in a fair way, we keep the amount of dynamics that produces the intervals equal in the generation of the ISIs. Figure 8 plots the NPE as a function of τ. Note that the NPE degrades as τ increases.

IV. HODGKIN AND HUXLEY MODEL NEURON

We used the approach of Sec. II for finding a feasible input region for a good reconstruction with the Hodgkin and Huxley (HH) [10] neuron model. This model is a four-variable system of nonlinear differential equations that reasonably accurately describes action potentials and their propagation. The Hodgkin and Huxley equations are

$$C\dot{v}=-g_{\mathrm{Na}}m^3h(v-E_{\mathrm{Na}})-g_{\mathrm{K}}n^4(v-E_K)-g_L(v-E_L)+S(t),$$

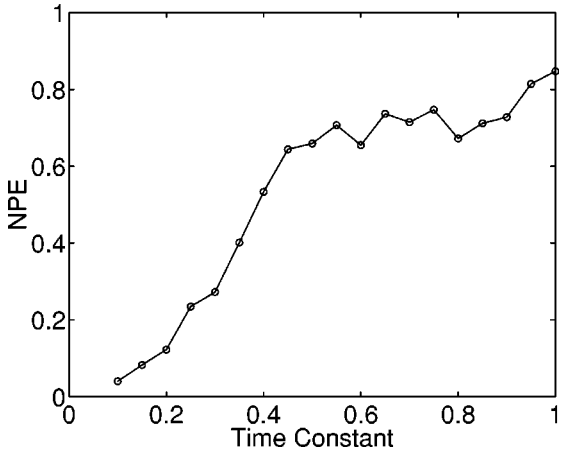

FIG. 8. Normalized one-step ahead prediction error of the ISIs generated with the FHN2 model and the Lorenz equations as a function of the time constant τ. Embedding dimension $m=3$. Input signal used: $S(t)=0.0035x(t)+0.26$.

$$\dot{m}=\alpha_m(v)(1-m)-\beta_m(v)m,$$

$$\dot{n}=\alpha_n(v)(1-n)-\beta_n(v)n,$$

$$\dot{h}=\alpha_h(v)(1-h)-\beta_h(v)h,$$

where $S(t)$ is an external input to a neuron and

$$\alpha_n(v)=\frac{0.01(10-v)}{\exp(10-v/10)-1},$$

$$\alpha_m(v)=\frac{0.1(25-v)}{\exp(25-v/10)-1},\quad \beta_h(v)=\frac{1}{\exp(30-v/10)+1},$$

$$\beta_m(v)=4\exp\left(\frac{-v}{18}\right),\quad \beta_n(v)=0.125\exp\left(\frac{-v}{80}\right),$$

$$\alpha_h(v)=0.07\exp\left(\frac{-v}{20}\right),$$

C is the capacitance; v is the membrane potential; the g's are constant conductances; $E_{\mathrm{Na}},E_{\mathrm{K}},E_L$ are constant equilibrium potentials; and m, h, and n are variables representing sodium activation, sodium inactivation, and potassium activation channels, respectively. (The parameters $E_{\mathrm{Na}}=50$, $E_{\mathrm{K}}=-77$, $E_L=-54.4$, $C=1$, $g_{\mathrm{Na}}=120$, $g_{\mathrm{K}}=36$, and $g_L=0.3$ were used in our calculations.)

Figure 9(a) shows the period-parameter plot for the Hodgkin and Huxley model. Note that the period is a monotonic function of S for $7\leqslant S\leqslant 150$. Any subset of this range will be an input scaling range that will produce good reconstructions. Figure 9(b) shows the delay embeddings of the ISIs generated with the HH model and $S(t)=2.5x(t)+70$, where $x(t)$ is the x coordinate of the Lorenz equations. This input signal results in an input range $20\leqslant S(t)\leqslant 120$. The ISIs were defined by upcrossing of the membrane potential variable v, and we set the threshold to -40. Note that the ISI attractor has the figure eight shape of the Lorenz attractor.

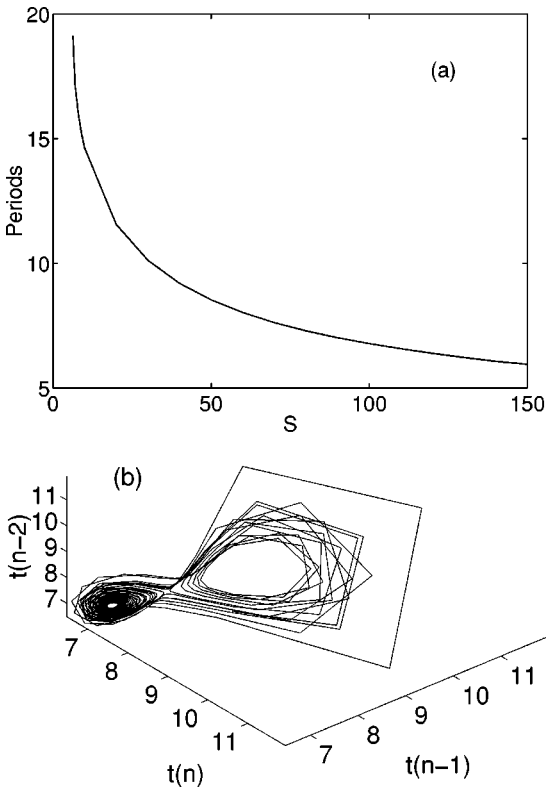

FIG. 9. (a) Period-parameter plot for the Hodgkin and Huxley model. (b) Plot of 3-tuples of interspike intervals generated with the Hodgkin and Huxley model and input signal $S(t)=2.5x(t)+70$, where $x(t)$ is the x coordinate of the Lorenz equations and $\tau=0.01$.

A sequence of 1024 ISIs generated as in Fig. 9(b) yields a very low NPE of 0.07, again reflecting a successful reconstruction. Prediction results for the original ISI series (lower curve) and the mean of ten sets of GS and RP surrogates (two upper curves) are shown in Fig. 10. The normalized one-step-ahead prediction error is plotted as a function of the embedding dimension m. For every value of m, the null hypotheses controlled by the surrogate data can be rejected, and we can conclude that there is nonlinear predictability in the ISI series.

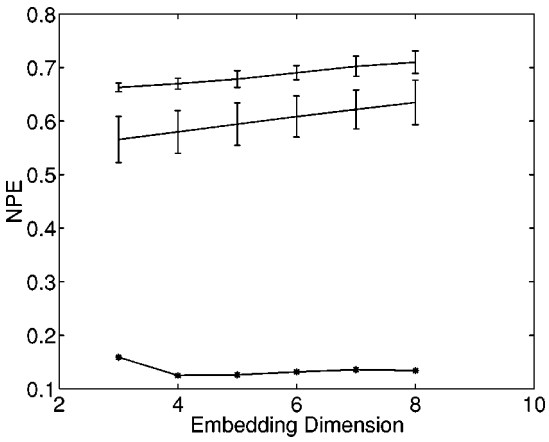

FIG. 10. NPE ($h=1,m=3$) as a function of embedding dimension. The lower curve is the NPE for the ISIs created with the Hodgkin and Huxley model and the Lorenz equations [as in Fig. 9(b)]; upper curve is the mean NPE of ten surrogate sets (phase-randomized surrogates, Gaussian-scaled surrogates). The error bars denote two standard deviations.

V. SUMMARY

We have considered ISI attractors generated by excitable neuron models subject to chaotic input signals. We have found that the period-parameter plot, which displays the dependence of the oscillation frequency of the spiking model on the input level, can be used to explain the success of reconstruction. The range of constant input signal where the periods are monotonic provides a scaling range for the chaotic input to the neuron model in which good reconstruction are obtained (from the point of view of geometry and nonlinear forecastability). By finding the monotonic input range and scaling the chaotic input to that range, we have successfully reconstructed attractors from neuron models. We have used the surrogate data method to verify that the nonlinear deterministic structure of the dynamics that produced the intervals is preserved in the ISIs.

ACKNOWLEDGMENT

The research of T.S. was supported in part by the National Science Foundation (Computational Mathematics and Physics Programs).

[1] N. Packard, J. Crutchfield, J. D. Farmer, and R. Shaw, Phys. Rev. Lett. **45**, 712 (1980).
[2] F. Takens, *Dynamical Systems and Turbulence*, Lecture Notes in Mathematics Vol. 898 (Springer-Verlag, Berlin, 1981).
[3] T. Sauer, J. A. Yorke, and M. Casdagli, J. Stat. Phys. **65**, 579 (1991).
[4] H. Tuckwell, *Introduction to Theoretical Neurobiology* (Cambridge University Press, Cambridge, 1988), Vols. 1 and 2.
[5] A. Rescigno, R. B. Stein, R. L. Purple, and R. E. Poppele, Bull. Math. Biophys. **32**, 337 (1970).
[6] B. W. Knight, J. Gen. Physiol. **59**, 734 (1972).
[7] L. Glass and M. C. Mackey, J. Math. Biol. **7**, 339 (1979).
[8] J. P. Keener, F. C. Hoppenstadt, and J. Rinzel, SIAM (Soc. Ind. Appl. Math.) J. Appl. Math. **41**, 503 (1981).
[9] R. FitzHugh, in *Biological Engineering*, edited by H. P. Schwann (McGraw-Hill, New York, 1962); J. Nagumo, S. Arimoto, and S. Yoshizawa, Proc. IRE **50**, 2061 (1962).
[10] A. L. Hodgkin and A. F. Huxley, J. Physiol. (London) **117**, 550 (1952).
[11] T. Sauer, Phys. Rev. Lett. **72**, 3811 (1994).
[12] D. M. Racicot and A. Longtin, Physica D **104**, 184 (1997).
[13] R. Castro and T. Sauer, Phys. Rev. Lett. **79**, 1030 (1997).
[14] O. E. Rössler, Phys. Lett. **57A**, 397 (1976).
[15] E. Lorenz, J. Atmos. Sci. **20**, 131 (1963).
[16] J. D. Farmer and J. J. Sidorowich, Phys. Rev. Lett. **59**, 845 (1987).

[17] T. Sauer and T. Sauer, in *Nonlinear Dynamics and Time Series*, edited by C. Cutler and D. Kaplan (American Mathematical Society, Providence, RI, 1996).

[18] S. J. Schiff, T. Sauer, and T. Chang, Integrative Physiol. Behav. Sci. **29**, 246 (1994).

[19] A. A. Tsonis and J. B. Elsner, Nature (London) **359**, 217 (1992).

[20] A. Longtin, Int. J. Bifurcation Chaos Appl. Sci. Eng. **3**, 651 (1993).

[21] J. Theiler, S. Eubank, A. Longtin, B. Galdrakian, and J. D. Farmer, Physica D **58**, 77 (1992).